The Astronomical Journal, 154:253 (16pp), 2017 December https://doi.org/10.3847/1538-3881/aa90b7

Radio Galaxy Zoo: A Search for Hybrid Morphology Radio Galaxies

A. D. Kapińska[1,2], I. Terentev[3], O. I. Wong[1,2], S. S. Shabala[4], H. Andernach[5], L. Rudnick[6], L. Storer[1], J. K. Banfield[2,7], K. W. Willett[6], F. de Gasperin[8], C. J. Lintott[9], Á. R. López-Sánchez[10,11], E. Middelberg[12], R. P. Norris[2,13,14], K. Schawinski[15], N. Seymour[16], and B. Simmons[9,17]

[1] International Centre for Radio Astronomy Research (ICRAR), University of Western Australia, 35 Stirling Highway, WA 6009, Australia; anna.kapinska@uwa.edu.au
[2] ARC Centre of Excellence for All-Sky Astrophysics (CAASTRO), Australia
[3] Zooniverse Citizen Scientist, c/o Oxford Astrophysics, Denys Wilkinson Building, Keble Road, Oxford OX1 3RH, UK
[4] School of Physical Sciences, University of Tasmania, Private Bag 37, Hobart, Tasmania 7001, Australia
[5] Depto. de Astronomía, DCNE, Universidad de Guanajuato, Apdo. Postal 144, Guanajuato, CP 36000, Gto., Mexico
[6] School of Physics and Astronomy, University of Minnesota, Minneapolis, MN 55455, USA
[7] Research School of Astronomy and Astrophysics, Australian National University, Canberra, ACT 2611, Australia
[8] Leiden Observatory, Leiden University, P.O. Box 9513, NL-2300 RA, Leiden, The Netherlands
[9] Astrophysics, Department of Physics, University of Oxford, Keble Road, Oxford OX1 3RH, UK
[10] Australian Astronomical Observatory, P.O. Box 915, North Ryde, NSW 1670, Australia
[11] Department of Physics and Astronomy, Macquarie University, NSW 2109, Australia
[12] Astronomisches Institut, Ruhr-Universität, Universitätsstr. 150, D-44801 Bochum, Germany
[13] CSIRO Australia Telescope National Facility, P.O. Box 76, Epping, NSW 1710, Australia
[14] Western Sydney University, Locked Bag 1797, Penrith South, NSW 1797, Australia
[15] Institute for Astronomy, Department of Physics, ETH Zurich, Wolfgang-Pauli-Strasse 27, CH-8093 Zurich, Switzerland
[16] International Centre for Radio Astronomy Research (ICRAR), Curtin University, Perth, Australia
[17] Center for Astrophysics and Space Sciences, Department of Physics, University of California, San Diego, CA 92093, USA
Received 2017 May 23; revised 2017 September 7; accepted 2017 September 28; published 2017 November 27

Abstract

Hybrid morphology radio sources (HyMoRS) are a rare type of radio galaxy that display different Fanaroff–Riley classes on opposite sides of their nuclei. To enhance the statistical analysis of HyMoRS, we embarked on a large-scale search of these sources within the international citizen science project, Radio Galaxy Zoo (RGZ). Here, we present 25 new candidate hybrid morphology radio galaxies. Our selected candidates are moderate power radio galaxies ($L_{\rm median} = 4.7 \times 10^{24}\,{\rm W\,Hz^{-1}\,sr^{-1}}$) at redshifts $0.14 < z < 1.0$. Hosts of nine candidates have spectroscopic observations, of which six are classified as quasars, one as high- and two as low-excitation galaxies. Two candidate HyMoRS are giant (>1 Mpc) radio galaxies, one resides at the center of a galaxy cluster, and one is hosted by a rare green bean galaxy. Although the origin of the hybrid morphology radio galaxies is still unclear, this type of radio source starts depicting itself as a rather diverse class. We discuss hybrid radio morphology formation in terms of the radio source environment (nurture) and intrinsically occurring phenomena (nature; activity cessation and amplification), showing that these peculiar radio galaxies can be formed by both mechanisms. While high angular resolution follow-up observations are still necessary to confirm our candidates, we demonstrate the efficacy of the RGZ in the pre-selection of these sources from all-sky radio surveys, and report the reliability of citizen scientists in identifying and classifying complex radio sources.

Key words: galaxies: active – galaxies: clusters: individual (WHL J122425.8+020310) – galaxies: jets – ISM: lines and bands – quasars: supermassive black holes – radio continuum: galaxies

1. Introduction

Hybrid morphology radio sources (hereafter HyMoRS) have been invoked in the debate on the origin of morphological dichotomy in radio galaxies since Gopal-Krishna & Wiita (2000) pointed out their existence. Gopal-Krishna & Wiita (2000) claimed that HyMoRS constitute a separate class of object alongside the large-scale radio galaxies of FR I and FR II types (Fanaroff & Riley 1974); the Fanaroff–Riley classes (FR) introduced over 40 years ago have proved to be a simple yet powerful tool in studies of radio galaxies.

In the original definition FR I and FR II radio sources were distinguished by the ratio, $\mathcal{R}$, of the distance between the brightness peaks of each side of the nucleus and the overall source size. If $\mathcal{R} < 0.5$, the radio source was classified as an FR I, otherwise as an FR II. Since the formulation of the FR classification, our understanding of radio galaxies has been evolving, both observationally and theoretically, and we now know that FR II radio galaxies exhibit tightly collimated and remarkably stable, often one-sided jets, which terminate forming well recognized features, the so-called hotspots. It is interpreted that the relativistic particles (either electron/proton or electron/positron pairs, see, e.g., De Young 2006) are re-accelerated in strong shocks at these jet termination points, and are further transported, through the backflow, into a cocoon encompassing the radio source (Blandford & Rees 1974; Scheuer 1974). FR Is, on the other hand, seem to display heavily turbulent jets; they are less well collimated and have been shown to decelerate while strongly interacting with the ambient medium soon after their ejection (Komissarov 1988; Laing & Bridle 2014).

The physical origin of the FR dichotomy in the radio galaxy population has been a widely debated issue for over 20 years

(e.g., Baum et al. 1992, 1995; De Young 1993; Reynolds et al. 1996a; Meier et al. 1997; Rawlings 2002; Kaiser & Best 2007; Kawakatu et al. 2009; Saripalli 2012; Gendre et al. 2013, among others). Theoretical works (Bicknell 1994, 1995; Kaiser & Best 2007; Kawakatu et al. 2009) explain the dichotomy in terms of power of the relativistic outflows, and deceleration and interaction of the jets with their environment. Such an interpretation has been supported by a wealth of observational studies (e.g., Hill & Lilly 1991; Zirbel 1997; Laing et al. 2011; Gendre et al. 2013; Thorat et al. 2013; Laing & Bridle 2014). Also, analytical solutions that link the transition of FR II sources into FR Is have been developed (Wang et al. 2011; Turner & Shabala 2015). On the other hand, some authors favor fundamental differences in the central engines of the two different FR classes as the interpretation of the dichotomy. For instance, through spectroscopic analysis of emission line nebulae associated with radio galaxies, Baum et al. (1992, 1995) suggested that the angular momentum of the accretion disk may be important in forming radio morphologies of extragalactic radio sources. Baum et al. suggested that the AGN in FR I radio galaxies are fed at low accretion rates and are possibly of low black hole spins, while those in FR II radio galaxies are expected to accrete at higher rates and be possibly of higher spins. Fundamental differences in the central engines of the two different FR classes are also favored by e.g., Meier et al. (1997) and Rawlings (2002). Differences in the particle composition of the jets have also been considered (e.g., Celotti & Fabian 1993; Reynolds et al. 1996b; Laing & Bridle 2002).

The current consensus is that the FR morphology is most likely due to a combination of jet power and the radio source environment (e.g., Best 2009; Saripalli 2012). HyMoRS, which —in simple terms—display FR I radio structures on one side of the nucleus and FR II on the other, seem to be a class of objects that may help us to disentangle the two effects. However, HyMoRS is a rare type of radio galaxy, with an estimated occurrence possibly as low as $<1\%$ of all extended radio galaxies (Gawroński et al. 2006). Here, we demonstrate how the Radio Galaxy Zoo project (RGZ; Banfield et al. 2015) is particularly useful in the search for HyMoRS.

This paper is structured as follows. We present the project and our data in Section 2. Our results, including notes on the RGZ candidate HyMoRS, their optical and radio properties, and performance of the RGZ project in classifying HyMoRS, are reported in Section 3. We discuss the possible origin of HyMoRS, their host galaxies, environments, and radio properties in Section 4. Summary and conclusions are given in Section 5. We assume a flat universe with a Hubble constant of $H_0 = 68$ km s^{-1} Mpc^{-1}, and $\Omega_\Lambda = 0.685$, and $\Omega_M = 0.315$ (Planck Collaboration et al. 2013) throughout the paper.

2. Observational Data

Our source of data for this work is the RGZ[18] citizen science project (Banfield et al. 2015). RGZ builds on the hugely successful Galaxy Zoo[19] (Lintott et al. 2008). RGZ uses major legacy radio and mid-IR large area surveys: the Faint Images of the Radio Sky at Twenty centimeters (FIRST; Becker et al. 1995), the Australia Telescope Large Area Survey (Norris et al. 2006), the *Wide-field Infrared Survey Explorer* (*WISE*; Wright et al. 2010), and the *Spitzer* Wide-Area Infrared Extragalactic Survey (SWIRE; Lonsdale et al. 2003).

2.1. RGZ Talk

In this paper, we present a sample of candidate hybrid morphology radio galaxies serendipitously identified by the RGZ citizen scientists, and discussed within the RGZ online forum, the RadioTalk.[20] In the standard process, the RGZ citizen scientists are provided with $3' \times 3'$ cut-outs drawn from the radio and mid-IR surveys that present them with a "subject" to classify. Their task is to (i) decide whether radio components in the FIRST cut-out are separate radio sources, or if they belong to one galaxy, and (ii) locate the mid-IR host galaxy of the radio source(s), if present, in the corresponding *WISE* image (for details, see Banfield et al. 2015). After the classification of each cut-out, the citizen scientists can discuss the subjects they have just classified with the RGZ science team members and other volunteers through the RadioTalk forum. We follow-up, with detailed visual inspection, radio sources tagged as having "hybrid" and "asymmetric" radio morphology and discussed by the volunteers on RadioTalk. In total, we inspected visually 427 sources, and the 25 best cases, all of which are reported in this paper, are considered strong HyMoRS candidates. However, the current sample cannot be used to give a quantitative estimate of the fraction of sources that fall into the HyMoRS category, because of the nonuniform way in which the sources are found. The pre-selection of the sources for RadioTalk by the volunteers is incidental, there is an unknown bias associated with which sources were tagged as hybrid or asymmetric, and a number of our candidates were found serendipitously by the science team.

2.2. RGZ Catalog

The first data release of the RGZ project (hereafter RGZ DR1) is based on the project's first 2.5 years of operation (O. I. Wong et al. 2017, in preparation). The RGZ DR1 catalog consists of over 74,000 radio source components from the FIRST survey, with a weighted consensus level of 65% or greater, where the consensus means here the level of agreement on the chosen mid-IR host and radio components of a subject being classified. A weighted consensus level of 65% results in a classification that is reliable at the 80%, or greater level (O. I. Wong et al. 2017, in preparation). Radio source classifications that are derived from the RadioTalk forum (such as those in this paper) are more likely to have greater reliability, since they stem from discussions between the citizen scientists and the science team. In this paper, we investigate all entries from the RGZ project pipeline of our candidate HyMoRS, including those entries that fall below the RGZ DR1 catalog consensus lower limit of 65%. For more details on the classification, see Banfield et al. (2015) and O. I. Wong et al. (2017, in preparation).

2.3. Multi-wavelength Cross-matching

We repeat the work of the citizen scientists and manually cross-match each selected RGZ radio source with the mid-IR *WISE* (3.4 μm band) and optical *r*-band (623 nm) Sloan Digital Sky Survey Data Release 13 (SDSS DR13; SDSS Collaboration et al. 2016) to verify the radio morphology of the sources, and to obtain redshift estimates. The manual selection of the

[18] http://radio.galaxyzoo.org/
[19] http://www.galaxyzoo.org/
[20] http://radiotalk.galaxyzoo.org/

mid-IR hosts allows us to cross-check the accuracy of the RGZ DR1 catalog specifically for future automated identification of HyMoRS candidates.

In addition, we cross-match our selected sources with radio surveys at other radio frequencies and angular resolution lower than that of the FIRST survey: the Galactic and Extragalactic All-Sky Murchison Widefield Array survey (GLEAM; Hurley-Walker et al. 2017) at 200 MHz, the NRAO Very Large Array (VLA) Sky Survey (NVSS; Condon et al. 1998) at 1.4 GHz, and the Green Bank 6 cm survey (GB6; Gregory et al. 1996) at 4.85 GHz. This procedure is to obtain total flux density measurements of our sources at 1.4 GHz, and an overall radio spectral index (α, where the flux density S at a frequency ν is $S_\nu \propto \nu^{-\alpha}$) for the radio luminosity density redshift correction.

3. Results

We select 25 candidate hybrid morphology radio galaxies. Our final sample is presented in Figures 1 and 2, where we plot radio contours from the FIRST survey over the *WISE* 3.4 μm-band images. In Tables 1 and 2, we list mid-IR and optical hosts of the radio galaxies, and provide radio, optical, and redshift information. In this section, we provide brief notes on our candidates (Section 3.1), present more detailed results on radio (Section 3.2) and optical (Section 3.3) properties of the candidates, and compare our results to the RGZ DR1 catalog (Section 3.4).

3.1. Notes on Candidate HyMoRS

1. *RGZ J023832.6+023349* (Figure 1(a)): In the FIRST image the NE lobe displays a strong hotspot-like component at its far end. The SW lobe is not detected in the FIRST image, but faint diffuse emission is detected in the NVSS image with no compact components present. A compact radio core detected in the FIRST image is coincident with a mid-IR host (Table 2). This is a giant (>1 Mpc) radio galaxy, with a size of almost 2 Mpc (based on work in Andernach et al. 2012), and one of the examples where the low angular resolution NVSS images are needed for the classification of the radio source. This source is a QSO at a spectroscopic redshift 0.209 (Schneider et al. 1994).

2. *RGZ J072406.7+380348* (Figure 2(a)): The SW lobe features a strong component, which can be considered a recessed hotspot, embedded in diffuse emission that links the hotspot to the radio core. The NE lobe has no dominant compact hotspot-like sources and is broken into separate components in the FIRST image. A compact radio core is detected. The host has targeted SDSS spectroscopic observations; located at $z = 0.241$ it is classified as a QSO.

3. *RGZ J082231.1+531118* (Figure 2(b)): The NW lobe displays a brightness peak at its far end, which can be considered a hotspot-like component, with emission extending toward the radio core. The SW lobe is plume-like extending in the S and SE directions. A radio core is detected, but at the angular resolution of FIRST it is merged with the diffuse emission of the SW lobe.

4. *RGZ J083352.2+045822* (Figure 2(c)): No radio core is detected, which makes the mid-IR host identification more difficult. In our interpretation the observed radio structure is that of a single radio galaxy with the mid-IR host *WISE* J083352.25 +045822.7. The NE lobe hosts a strong hotspot-like component at its northernmost end. The SW lobe displays elongated, relaxed structure. We note that the structure could be also interpreted as coming from two separate radio galaxies, but in such a case the northern source would be composed of a single lobe with no distinguishable radio core. No additional low-level emission that could be associated to a potential southern lobe in such an alternative interpretation is detected in the NVSS image.

5. *RGZ J084738.0+183158* (Figure 2(d)): The side NE from the radio core is a strong, compact component, which could be considered a hotspot. There is an optical object (with no mid-IR counterpart) in the vicinity that could be, in principle, associated with the NE component; however, the object seems to be detected in the SDSS images only, and it is classified within SDSS as a star. The SW lobe displays a tail-like, relaxed structure. A radio core is detected coincident with a faint mid-IR host. We found no optical or X-ray counterpart of the host in the publicly available surveys. However, there is a noncataloged object 4 arcsec SE from the mid-IR host detected in the Digitized Sky Survey red image that potentially could be the optical counterpart. This radio galaxy is our weakest candidate HyMoRS, as there is a possibility the NE component is an unassociated infrared faint radio source (IFRS; Collier et al. 2014).

6. *RGZ J085926.7+292738* (Figure 2(e)): The southern lobe features a strong, hotspot-like component at its far end, with diffuse emission extending between the strong component and the radio core. The northern lobe is devoid of any strong compact component, displaying only diffuse emission similar to the lobe emission of the southern lobe. A compact radio core is detected, embedded in the diffuse lobe emission.

7. *RGZ J091408.0+522948* (Figure 2(f)): The eastern lobe is dominated by a hotspot-like component. The western lobe displays elongated plume-like emission with a surface brightness decreasing with distance from the core. A compact radio core is detected.

8. *RGZ J094214.2+062751* (Figure 2(g)): The emission of the SW lobe is uniform along its whole extent, displaying a confined structure. If a hotspot is present, it is merged with the lobe emission. The NE lobe consists of an elongated, tail-like diffuse emission with the brightness peak in the inner part of the lobe, and shows a relaxed structure. A radio core is not easily distinguished and, if present, it is merged with the southern lobe of the source.

9. *RGZ J103435.8+251817* (Figure 2(h)): The western lobe has a strong, hotspot-like component at its far end, with diffuse lobe emission pointing toward the radio core. The eastern lobe is devoid of any strong, compact components, and its diffuse emission seems to bend toward the south. A radio core is detected, but is merged with the eastern lobe. The host has targeted SDSS Baryon Oscillation Spectroscopic Survey (SDSS BOSS; SDSS Collaboration et al. 2016) observations; located at $z = 0.3941$ it is classified as a luminous red galaxy. This object is a high excitation radio galaxy (HERG; see Section 3.3).

10. *RGZ J105521.2+372652* (7C 1052+3742; Figure 2(i)): The northern lobe is dominated by a hotspot-like component. The southern lobe consists of an elongated diffuse emission of a relaxed structure. A compact radio core is detected. The host has targeted SDSS spectroscopic observations; located at $z = 0.5886$ it is classified as a QSO.

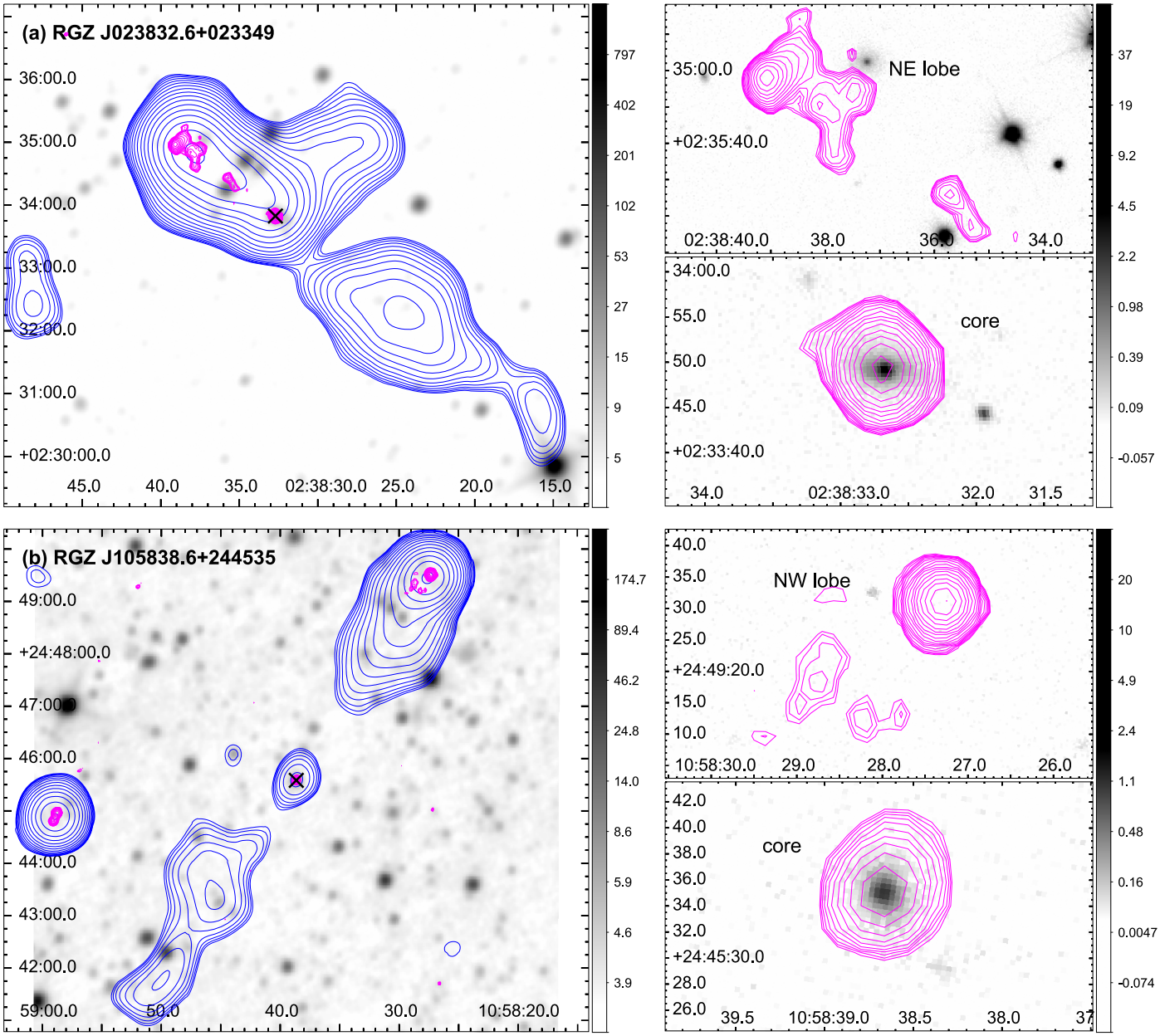

Figure 1. Left: *WISE* 3.4 μm images with overlaid FIRST (magenta) and NVSS (blue) of two giant candidate HyMoRS for which inspection of the NVSS image was necessary. The contours are drawn at levels $3\sigma + \sigma \times 2^{n/2}$ for $n \geqslant 0$, and where $\sigma = 0.15$ mJy beam^{-1} (FIRST) and $\sigma = 0.45$ mJy beam^{-1} (NVSS). *WISE*: the colorbars are in log scale and are in the raw intensity units of DN/pixel. Hosts of the radio galaxies are marked with crosses. Right: zoom in on components detected in FIRST overlaid on SDSS DR13 r' band images. The FIRST contours are at the same level as in the left panel images. The colorbars are in log scale and are in the SDSS units of nanomaggies (http://www.sdss.org/dr13/algorithms/magnitudes/).

11. *RGZ J105838.6+244535* (Figure 1(b)): In the FIRST image the NW lobe displays a strong hotspot-like component at its far end. The SE lobe is resolved out in FIRST, but its diffuse emission is detected in the lower resolution NVSS image. There is no compact component in the SE lobe, and its overall structure seems relaxed. A compact radio core is detected in the FIRST image. This is a giant radio galaxy, with a size of 2.3 Mpc (Dabhade et al. 2017).

12. *RGZ J120343.7+234304* (Figure 2(j)): The NW lobe is dominated by a bright, albeit extended at FIRST angular resolution of 5.″4, hotspot-like component. In the NVSS image no radio emission is detected beyond that detected in FIRST. The SE lobe consists of a pointed tail-like emission that distorts and bends in the outer parts of the lobe. A faint radio core is detected. The host has targeted SDSS spectroscopic observations; located at $z = 0.1767$ the galaxy is a low excitation radio galaxy (LERG; see Section 3.3).

13. *RGZ J122425.8+020310* (Figure 2(k)): The eastern lobe displays a strong hotspot-like component at its far end, with lobe emission pointing back toward the host galaxy. Some of the lobe emission close to the hotspot-like component extends sideways, to the north. The western lobe is devoid of any strong compact component, but it is rather straight becoming more extended sideways at the lobe far end. If a radio core is

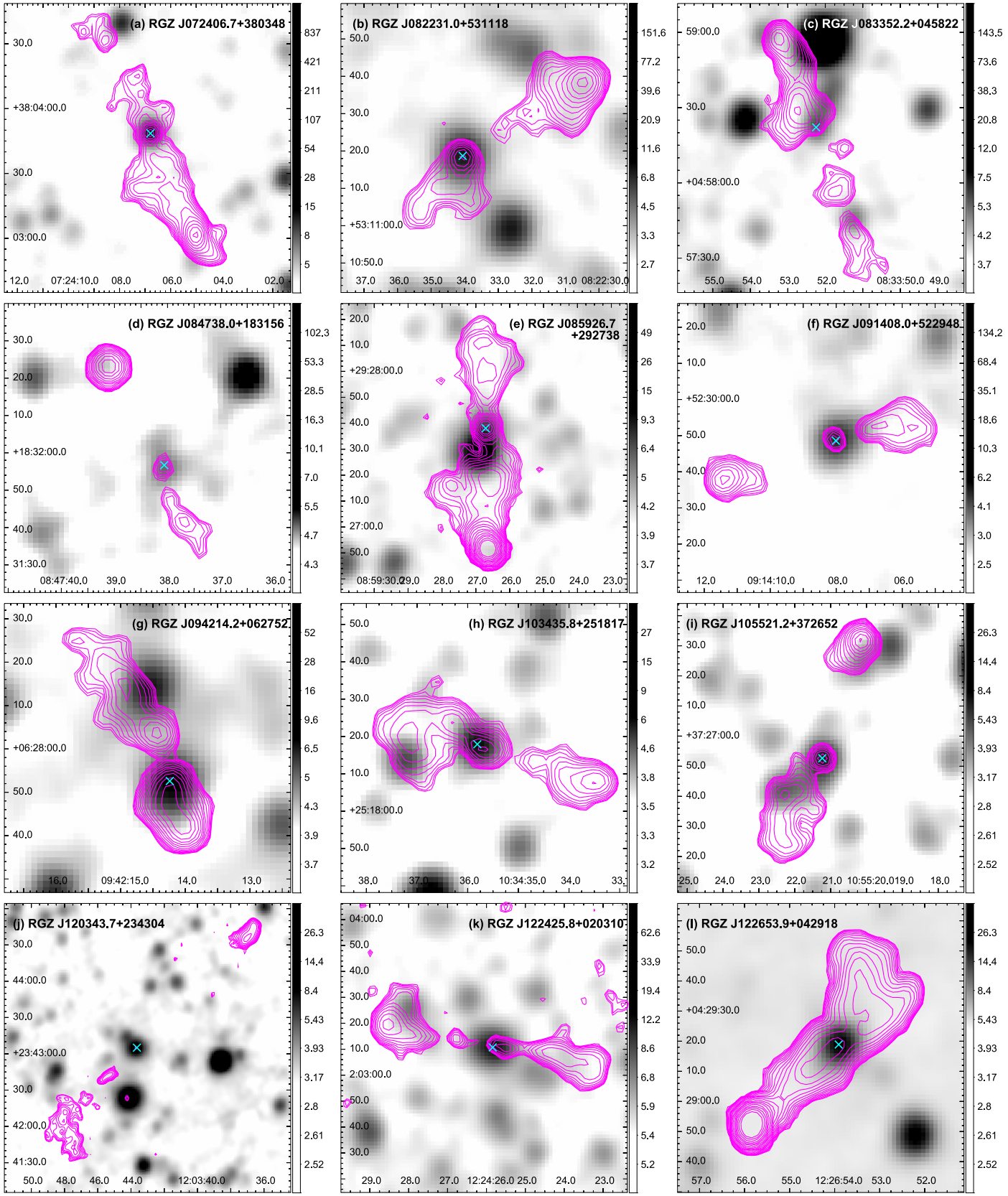

Figure 2. *WISE* 3.4 μm images of candidate HyMoRS with overlaid FIRST contours. Hosts of the radio galaxies are marked with crosses. The FIRST contours are drawn at levels $3\sigma + \sigma \times 2^{n/2}$ for $n \geqslant 0$, and where $\sigma = 0.15$ mJy beam^{-1}. The colorbars are in log scale and are in the raw intensity units of DN/pixel. For RGZ J123300.2+060325 we additionally include a true color SDSS image of its rare green bean galaxy host (panel (m)).

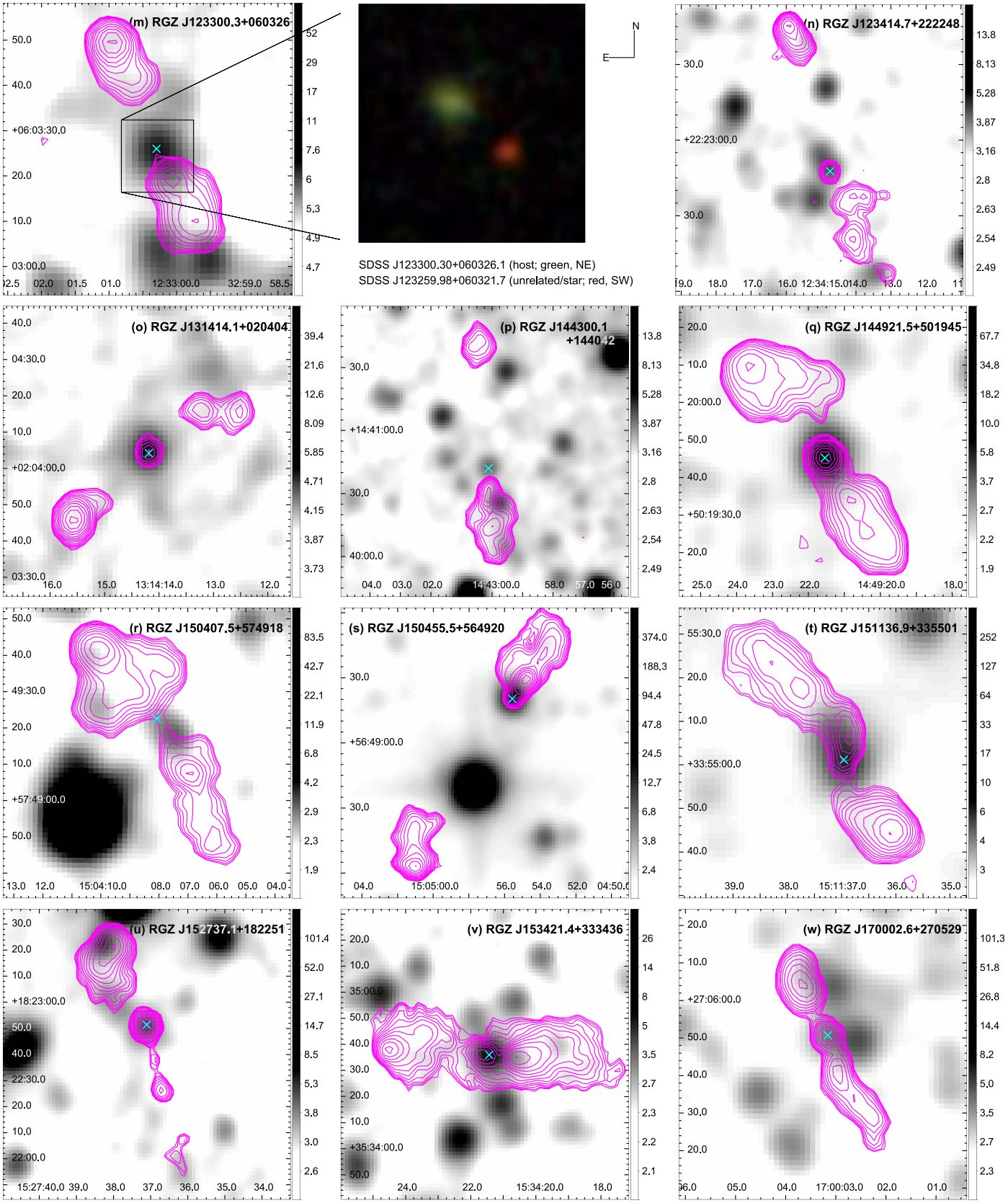

Figure 2. (Continued.)

Table 1
Optical Hosts of Candidate RGZ HyMoRS

HyMoRS name	R.A. (J2000)	Decl. (J2000)	m_r	m_R	M_R	z	z_{err}	z_{type}
RGZ J023832.6+023349	02 38 32.67	+02 33 49.2	17.14 ± 0.01	17.06 ± 0.02	−22.86 ± 0.02	0.209	0.001	spectro[a]
RGZ J072406.7+380348	07 24 06.79	+38 03 48.6	17.70 ± 0.01	17.70 ± 0.02	−22.31 ± 0.02	0.2414	0.00002	spectro
RGZ J082231.0+531118	08 22 34.06	+53 11 18.7	18.18 ± 0.04	18.18 ± 0.07	−20.81 ± 0.08[c]	0.138	0.011	photo
RGZ J083352.2+045822	08 33 52.25	+04 58 22.4	19.58 ± 0.03	19.82 ± 0.24	−20.31 ± 0.32[c]	0.227	0.114	photo[b]
RGZ J084738.0+183156	…	…	…	…	…	…	…	…
RGZ J085926.7+292738	08 59 26.71	+29 27 38.1	18.86 ± 0.02	19.53 ± 0.05	−20.87 ± 0.07	0.272	0.021	photo
RGZ J091408.0+522948	09 14 08.01	+52 29 48.6	20.97 ± 0.11	20.97 ± 0.27	−20.86 ± 0.28	0.607	0.039	photo
RGZ J094214.2+062752	09 42 14.24	+06 27 52.4	18.94 ± 0.02	19.41 ± 0.24	−21.52 ± 0.24	0.359	0.023	photo
RGZ J103435.8+251817	10 34 35.81	+25 18 17.9	19.86 ± 0.04	19.51 ± 0.06	−22.21 ± 0.06	0.39481	0.00002	spectro
RGZ J105521.2+372652	10 55 21.24	+37 26 52.6	18.78 ± 0.01[d]	18.32 ± 0.02	−24.34 ± 0.02	0.58858	0.00006	spectro
RGZ J105838.6+244535	10 58 38.66	+24 45 35.1	17.94 ± 0.01	18.05 ± 0.02	−21.78 ± 0.04	0.201	0.016	photo
RGZ J120343.7+234304	12 03 43.71	+23 43 04.7	16.66 ± 0.01	16.70 ± 0.02	−22.88 ± 0.02	0.1767	0.00005	spectro
RGZ J122425.8+020310	12 24 25.84	+02 03 10.7	18.59 ± 0.02	18.66 ± 0.05	−22.92 ± 0.05	0.45157	0.00007	spectro
RGZ J122653.9+042918	12 26 53.91	+04 29 18.9	19.47 ± 0.02	19.32 ± 0.04	−22.65 ± 0.04	0.51743	0.00002	spectro
RGZ J123300.2+060325	12 33 00.30	+06 03 26.1	19.16 ± 0.02	19.08 ± 0.04	−21.80 ± 0.11	0.269	0.058	photo
RGZ J123414.7+222248	12 34 14.73	+22 22 47.9	23.13 ± 0.56	…[e]	…[e]	0.881	0.052	photo
RGZ J131414.1+020404	13 14 14.19	+02 04 04.3	21.45 ± 0.13	21.52 ± 0.41	−22.22±0.43[f]	0.982	0.086	photo
RGZ J144300.1+144042	14 43 00.11	+14 40 42.1	20.26 ± 0.04	20.90 ± 0.13	−20.58 ± 0.15	0.425	0.041	photo
RGZ J144921.5+501945	14 49 21.53	+50 19 45.3	19.20 ± 0.02	19.30 ± 0.04	−21.71 ± 0.11	0.329	0.061	photo
RGZ J150407.5+574918	15 04 08.08	+57 49 22.5	20.28 ± 0.03	20.04 ± 0.07	−21.98 ± 0.11	0.465	0.051	photo
RGZ J150455.5+564920	15 04 55.56	+56 49 20.3	19.92 ± 0.03	20.36 ± 0.18	−20.57 ± 0.18	0.35871	0.00004	spectro
RGZ J151136.9+335501	15 11 36.93	+33 55 01.1	20.36 ± 0.06	20.18 ± 0.08	−23.01±0.08[f]	0.62341	0.00020	spectro
RGZ J152737.1+182250	15 27 37.11	+18 22 51.3	20.50 ± 0.10	21.11 ± 0.27	−20.14 ± 0.29	0.445	0.074	photo
RGZ J153421.4+333436	15 34 21.43	+33 34 35.9	18.15 ± 0.01	18.25 ± 0.02	−21.70 ± 0.04	0.210	0.015	photo
RGZ J170002.6+270549	17 00 03.15	+27 05 50.6	20.69 ± 0.12	20.64 ± 0.19	−22.24 ± 0.19[f]	0.719	0.032	photo

Notes. Redshifts, optical positions, and *r*-band Cmodel magnitudes, corrected for galactic extinction and transformed into *R*-band (Jester et al. 2005), are sourced from the SDSS DR13 unless stated otherwise.
[a] Schneider et al. (1994).
[b] Average of the SDSS DR13 (KD-tree method), SDSS DR10 (RF method), Brescia et al. (2014), and Bilicki et al. (2016) estimates.
[c] Calculated with SDSS *g*-band magnitude that has been verified with the Pan-STARRS measurement (Finkbeiner et al. 2016; Flewelling et al. 2016).
[d] Quasar, psf magnitude used.
[e] Unreliable *g*-band magnitude.
[f] Lower limit, correct value of k-correction unavailable due to high redshift of the galaxy.

present, it is merged with the western lobe emission. The host has targeted SDSS BOSS spectroscopic observations; located at $z = 0.4516$ the galaxy is an LERG (see Section 3.3). The host of this radio galaxy is the brightest cluster galaxy (BCG) of a galaxy cluster WHL J122425.8+020310 (Wen et al. 2009, this is a new estimate of the cluster redshift, improving on the original photometric estimate).

14. *RGZ J122653.9+041918* (4C + 04.43; Figure 2(l)): The SE lobe is dominated by a hotspot-like component. This component has been previously interpreted as a compact radio core, but no optical (SDSS) nor infrared (*WISE*) counterparts are found in its vicinity, and no radio variability has been found (Gorshkov & Konnikova 1995; Ofek & Frail 2011). The NW lobe displays a bifurcation extending north and northwest. We note this is a re-discovery, since the source has been marked previously by Proctor (2011) as a possible HyMoRS. If a radio core is present, it is merged with the diffuse lobe emission. The host has targeted SDSS spectroscopic observations; located at $z = 0.5174$ it is classified as a QSO.

15. *RGZ J123300.2+060325* (Figure 2(m)): The NE lobe displays a hotspot-like component at its far end, with extended emission pointing back toward the host galaxy. The SW lobe is more relaxed, with no clear compact component. No radio core is detected.

16. *RGZ J123414.7+222248* (7C 1231+2239; Figure 2(n)): The northern lobe is dominated by a strong hotspot-like component. The southern lobe displays diffuse meandering emission. A compact radio core is detected.

17. *RGZ J131414.1+020404* (Figure 2(o)): The SE lobe displays a strong hotspot-like component, with low-level emission pointing toward the radio core. The NW lobe is bent and is of a tail-like structure. A compact radio core is detected.

18. *RGZ J144300.1+144042* (Figure 2(p)): The northern lobe displays a bright component, which is resolved at the FIRST angular resolution of 5.″4. No additional emission is detected in NVSS beyond the FIRST component. The southern lobe displays elongated diffuse emission. No radio core is detected. This source is, to some degree, reminiscent of the HyMoRS reported by Pirya et al. (2011).

19. *RGZ J144921.5+501945* (Figure 2(q)): The NE lobe displays a strong hotspot-like component at its far end, with lobe diffuse emission extending both toward the radio core and sideways, perhaps representing a backflow. The SW lobe has no hotspot-like components, and its brightest peak is located close to the radio core. A compact radio core is detected. This radio galaxy has been previously classified as a possible BL Lac object (D'Abrusco et al. 2014).

20. *RGZ J150407.5+574918* (Figure 2(r)): The NE lobe displays a hotspot-like component at its far end, and more diffuse lobe emission pointing toward the position of the host galaxy, but also extending somewhat sideways. The SW lobe is of a plume-like, relaxed, and meandering structure. No clear

Table 2
Mid-IR Hosts and Radio Luminosity Densities of Candidate RGZ HyMoRS

HyMoRS Name	All *WISE* Host Name	$S_{\rm GLEAM}$ (mJy)	$S_{\rm NVSS}$ (mJy)	$S_{\rm GB6}$ (mJy)	$L_{\rm NVSS}$ ($\times 10^{24}$ W Hz^{-1} sr^{-1})	α
RGZ J023832.6+023349	J023832.67+023349.0	1600 ± 160	438.1 ± 11.9	128 ± 12	4.85 ± 0.13	0.79 ± 0.06
RGZ J072406.7+380348	J072406.79+380348.6	⋯	323.5 ± 10.5	77 ± 7	4.60 ± 0.15	1.16 ± 0.08
RGZ J082234.0+531118	J082234.06+531118.9	⋯	75.7 ± 2.6	35 ± 5	0.34 ± 0.01	0.62 ± 0.12
RGZ J083352.2+045822[a]	J083352.24+045822.6	532 ± 43	149.9 ± 5.1	39 ± 6	2.02 ± 0.28	0.76 ± 0.07
RGZ J084738.0+183156	J084738.07+183156.2	178 ± 23	24.5 ± 1.2	⋯	⋯	1.02 ± 0.07
RGZ J085926.7+292738	J085926.73+292738.1	1847 ± 240	547.1 ± 15.7	176 ± 16	11.22 ± 0.42	0.75 ± 0.06
RGZ J091408.0+522948	J091408.03+522948.7	⋯	30.9 ± 1.5	⋯	4.45 ± 0.27	⋯
RGZ J094214.2+062752[a]	J094214.21+062751.9	265 ± 21	81.0 ± 2.8	⋯	3.34 ± 0.14	0.61 ± 0.04
RGZ J103435.8+251817	J103435.81+251817.8	263 ± 34	62.0 ± 2.5	⋯	3.09 ± 0.12	0.74 ± 0.07
RGZ J105521.2+372652	J105521.24+372652.4	⋯	92.5 ± 2.5	30 ± 4	11.44 ± 0.31	0.91 ± 0.11
RGZ J105838.6+244535	J105838.67+244535.0	886 ± 109	158.5 ± 4.9	…[b]	1.58 ± 0.06	0.88 ± 0.07
RGZ J120343.7+234304	J120343.72+234304.6	1586 ± 206	430.3 ± 10.4	81 ± 8	3.18 ± 0.08	0.95 ± 0.13
RGZ J122425.8+020311	J122425.83+020310.6	417 ± 33	69.8 ± 2.1	⋯	4.52 ± 0.14	0.92 ± 0.04
RGZ J122653.9+041918	J122653.90+042918.9	2717 ± 217	688.9 ± 21.7	245 ± 23	66.52 ± 2.10	0.75 ± 0.02
RGZ J123300.2+060325	J123300.28+060325.6	245 ± 20	42.6 ± 1.7	⋯	0.82 ± 0.06	0.90 ± 0.05
RGZ J123414.7+222248	J123414.79+222248.9	349 ± 45	63.4 ± 1.9	22 ± 4	21.82 ± 1.23	0.87 ± 0.01
RGZ J131414.1+020404	J131414.19+020404.6	216 ± 17	47.8 ± 1.9	⋯	23.00 ± 2.01	0.78 ± 0.05
RGZ J144300.1+144042	J144300.11+144042.2	442 ± 35	91.2 ± 2.6	35 ± 5	5.33 ± 0.24	0.80 ± 0.01
RGZ J144921.5+501945	J144921.52+501945.7	⋯	137.7 ± 5.0	44 ± 5	4.21 ± 0.32	0.92 ± 0.10
RGZ J150407.5+574918[a]	J150407.50+574918.0	⋯	97.5 ± 3.5	⋯	7.23 ± 0.46	⋯
RGZ J150455.5+564920	J150455.56+564920.5	⋯	118.6 ± 4.5	61 ± 6	4.99 ± 0.19	0.54 ± 0.08
RGZ J151136.9+335501	J151136.94+335501.1	⋯	65.6 ± 2.3	21 ± 4	9.29 ± 0.33	0.92 ± 0.16
RGZ J152737.1+182250	J152737.11+182250.7	679 ± 54	143.5 ± 4.9	72 ± 7	9.66 ± 0.81	0.72 ± 0.05
RGZ J153421.4+333436	J153421.42+333436.0	⋯	239.8 ± 8.2	85 ± 8	2.67 ± 0.10	0.83 ± 0.08
RGZ J170002.6+270549[a]	⋯	⋯	54.2 ± 2.0	⋯	11.96 ± 0.57	⋯

Notes. $S_{\rm GLEAM/NVSS/GB6}$ are integrated flux densities as measured in the GLEAM (200 MHz), NVSS (1.4 GHz), or GB6 (4.85 GHz) surveys. $L_{\rm NVSS}$ is the rest frame total luminosity density of the source at 1.4 GHz, and α is the spectral index (simple power-law) calculated from the GLEAM, NVSS, and/or GB6 data.
[a] Host uncertain or confused in the *WISE* image.
[b] Only one lobe detected.

radio core is detected, but the host is most likely SDSSJ150408.08+574922.5. The mid-IR counterpart is confused with a nearby galaxy.

21. *RGZ J150455.5+564920* (Figure 2(s)): The SE lobe displays a strong hotspot-like component, with extended emission bent and pointing toward the direction of the host galaxy. The NW lobe is of more extended, diffuse, and relaxed structure, with brightness peak occuring close to the position of the host galaxy. If a radio core is present, it is merged with the NW lobe emission. The host has targeted SDSS spectroscopic observations; located at $z = 0.3587$, it is classified as a broadline QSO.

22. *RGZ J151136.9+335501* (7C 1509+3406; Figure 2(t)): The SW lobe displays a hotspot-like component with diffuse lobe emission pointing eastward. The NE lobe is of a plume-like structure. A radio core is not easily distinguishable, and if present it is merged with the diffuse emission connecting the lobes of the radio galaxy. The host has targeted SDSS spectroscopic observations; located at $z = 0.6234$, it is classified as a QSO.

23. *RGZ J152737.1+182250* (Figure 2(u)): The NE lobe displays a hotspot-like component at its far end, with extended emission bending and extending south, but slightly pointing toward the radio core. The SW lobe features a brightness peak in the proximity of the strong radio core, with some detached emission further away. A strong, compact radio core is detected.

24. *RGZ J153421.4+333436* (7C 1532+3344; Figure 2(v)): The eastern lobe features a strong hotspot-like component at its far end, with diffuse lobe emission extending between the hotspot and the radio core. The western lobe features a brightness peak close to the radio core, and displays diffuse emission extending far beyond the brightness peak, away from the radio core. A radio core is detected, but is embedded in the diffuse lobe emission.

25. *RGZ J170002.6+270549* (Figure 2(w)): The NE lobe features a single, but somewhat extended strong component. The SW lobe is devoid of compact components and consists of a tail-like structure slightly meandering away from the radio core. A radio core is detected.

3.2. Radio Properties

We measure the total radio luminosity density at 1.4 GHz, the radio spectral index between 200 MHz and 4.85 GHz, and the total projected linear extent of each of our candidate HyMoRS. Results are presented in Tables 1 and 2. The radio luminosity densities are k-corrected using the measured radio spectral index (unless unavailable, in which case the canonical $\alpha = 0.75$ is used). The total projected linear extent is measured between the outermost 3σ contours in the FIRST images (Scheuer 1995). The results are plotted in Figure 3, and further discussed in Section 4.3.

Although our candidates remain selected solely on the basis of visual inspection, to attempt a quantitative assessment of radio morphology of the candidates in this paper, we calculate the $f_{\rm FR}$ index (Krause et al. 2012) that stems directly from the

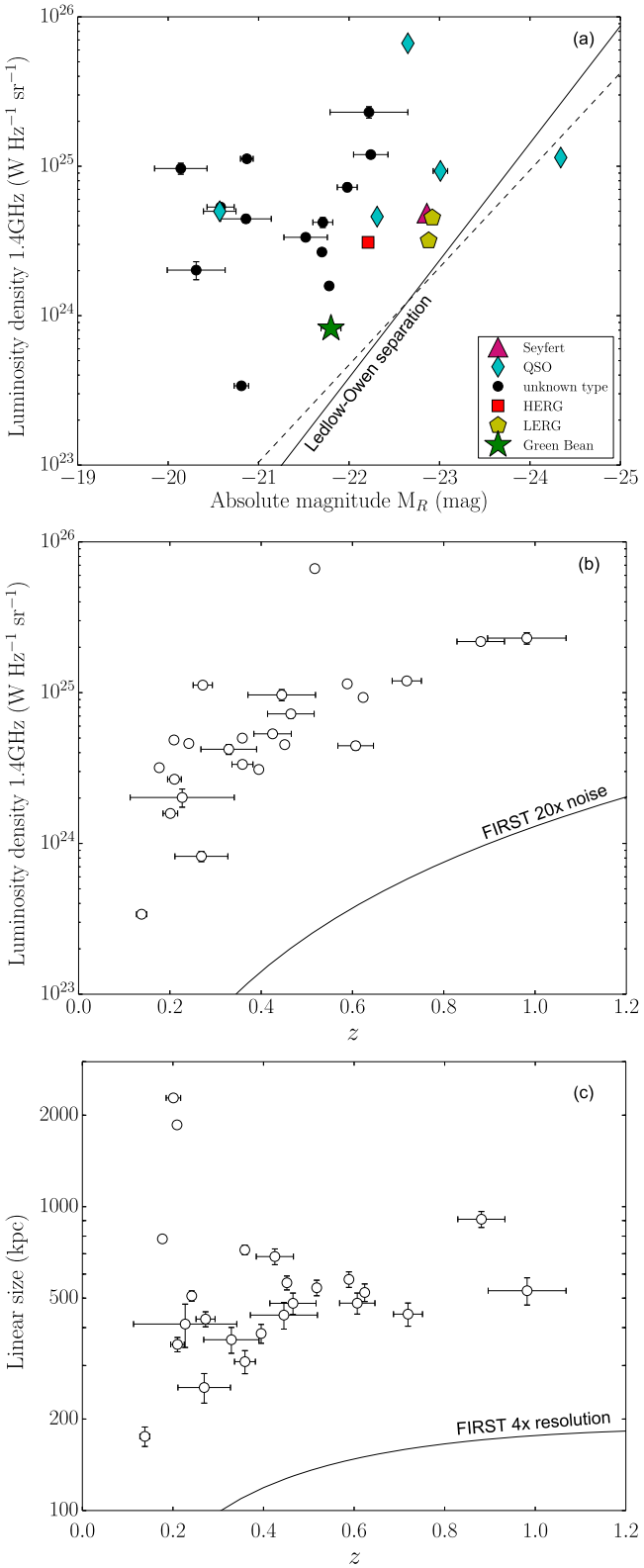

Figure 3. (a) Ledlow–Owen diagram for the RGZ HyMoRS candidates. The solid line indicates the separation of FRI and FRII sources proposed by Ledlow & Owen (1996), and the dashed line the separation of FRIs and FRIIs updated by Gopal-Krishna & Wiita (2001). (b) Luminosity density—redshift distribution. The luminosity density equal to 20σ FIRST noise level (3 mJy) is drawn for reference. (c) Linear size—redshift distribution. The linear size equal to $4\times$ FIRST resolution ($20''$) is drawn for reference. For a discussion, see Section 4.3.

original Fanaroff & Riley (1974) FR definition

$$f_{\rm FR} = \frac{2x_{\rm bright}}{x_{\rm total}} + 0.5, \quad (1)$$

where $x_{\rm bright}$ is the distance of the brightest pixel in the lobe from the position of the host, and $x_{\rm total}$ is the distance between the position of the optical host and farthest extent of the lobe. Following Krause et al. (2012), if $0.5 \leqslant f_{\rm FR} \leqslant 1.5$, the lobe is of an FRI morphology, and if $1.5 < f_{\rm FR} \leqslant 2.5$ the lobe is considered that of an FRII morphology. There are a few caveats associated with the use of this definition, however. For example, the index value will be overestimated if the extended emission in the outer parts of the lobe is resolved out due to shortcomings of the observations. The FIRST survey is particularly susceptible to this effect because of the lack of short baselines. Also, this method works best when a lobe hosts a clear brightness peak; however, the index may be misleading when the surface brightness emission of the lobe displays little variation with distance from the core. Therefore, the index should be considered an indication rather than a strict classification method. We measure the $f_{\rm FR}$ index for each lobe of each HyMoRS candidate. We use the FIRST survey for the $x_{\rm bright}$ and $x_{\rm total}$ measurements (unless otherwise stated in the results table) and the results are presented in Table 3.

The FR II sides of all candidate HyMoRS in this paper are quantified as such with Equation (1) ($f_{\rm FR} > 1.5$). In the case of the FR I sides, four candidates show index values of $1.68 \leqslant f_{\rm FR} \leqslant 2.02$, which in principle classifies them as of an FR II morphology. In the case of RGZ J072406.7+380348 (Figure 2(a); $f_{\rm FR} = 2.02 \pm 0.07$ for the FR I side) and RGZ J084738.0+183156 (Figure 2(d); $f_{\rm FR} = 1.79 \pm 0.17$ for the FR I side) there is a possibility that faint low surface brightness emission extending further away is resolved out in the FIRST images, causing $x_{\rm total}$ to be underestimated. RGZ J122425.8+020310 (Figure 2(k); $f_{\rm FR} = 1.78 \pm 0.10$ for the FR I side) displays a plateau-like emission (as opposed to peaked) across more than 50% of the lobe extent. We also note that, given the uncertainties, the FR indices of RGZ J084738.0+183156, RGZ J122425.8+020310, and RGZ J131414.1+020404 (Figure 2(d), (k), (o)) are all borderline cases.

Although the $f_{\rm FR}$ formula is based on the definition of FRI and FRII morphology, we additionally verified the range of the index values for typical FRIs and FRIIs. We selected extended radio galaxies from the 3CRR catalog (Laing et al. 1983) that were located at redshifts $z < 1.0$ and within the FIRST survey coverage. The 3CRR radio galaxies are powerful radio sources, but weaker sources have not been studied as extensively and radio morphology classification of 3CRR radio galaxies is very secure. For consistency, we use the FIRST survey images to measure the $f_{\rm FR}$ index of the 3CRR sources. We find that the average $f_{\rm FR}$ index for lobes of FRI radio sources is 1.13 ± 0.29, with a median of 1.17 (6 radio sources, 12 measurements). There is only one lobe of one FRI radio galaxy that is an outlier with $f_{\rm FR} = 1.57 \pm 0.13$. For FRII radio sources, the average $f_{\rm FR}$ index is 2.13 ± 0.28, with a median of 2.24, and all lobes of FRII sources have $f_{\rm FR} > 1.49$ (11 radio sources, 22 measurements).

Table 3
Radio Properties of Candidate HyMoRS

HyMoRS Name	f_{FR} / FRI Side	f_{FR} / FRII Side	θ_{FRI} (arcsec)	θ_{FRII} (arcsec)	θ_{total} (arcsec)	D_{total} (kpc)
RGZ J023832.6+023349	1.39 ± 0.07[a]	2.35 ± 0.04	355[a]	170[a]	530[a]	1860 ± 20
RGZ J072406.7+380348	2.02 ± 0.07 (0.50 ± 0.01)	2.07 ± 0.07	61	69	130	510 ± 20
RGZ J082234.0+531118	0.96 ± 0.24 (0.50 ± 0.01)	2.18 ± 0.10	25	47	70	175 ± 15
RGZ J083352.2+045822	1.33 ± 0.07	2.26 ± 0.10	65	47	110	410 ± 65
RGZ J084738.0+183156	1.79 ± 0.17	2.20 ± 0.12	27	38	65	...
RGZ J085926.7+292738	1.58 ± 0.09 (0.50 ± 0.01)	2.23 ± 0.08	49	56	100	470 ± 25
RGZ J091408.0+522948	1.43 ± 0.16	2.21 ± 0.12	29	40	70	480 ± 40
RGZ J094214.2+062751	1.02 ± 0.13	1.61 ± 0.27	43	18	60	310 ± 25
RGZ J103435.8+251817	1.17 ± 0.18 (0.50 ± 0.01)	2.21 ± 0.12 (0.60 ± 0.43)	29	38	70	380 ± 25
RGZ J105521.2+372652	1.45 ± 0.12	2.20 ± 0.09	40	51	85	575 ± 35
RGZ J105838.6+244535	1.50 ± 0.05[a]	2.18 ± 0.05[a]	340[a]	330[a]	670[a]	2280 ± 55
RGZ J120343.7+234304	1.17 ± 0.04	2.27 ± 0.03	110	145	255	785 ± 15
RGZ J122425.8+020310	1.78 ± 0.10	2.27 ± 0.09	47	49	95	560 ± 30
RGZ J122653.9+041918	1.55 ± 0.13	2.13 ± 0.09	36	51	85	540 ± 30
RGZ J123300.2+060325	1.07 ± 0.20	2.15 ± 0.14	27	33	60	255 ± 30
RGZ J123414.7+222248	1.57 ± 0.09	2.33 ± 0.07	52	67	115	910 ± 55
RGZ J131414.1+020404	1.68 ± 0.14 (0.50 ± 0.10)	2.18 ± 0.13	36	36	65	530 ± 55
RGZ J144300.1+144042	1.06 ± 0.11	2.24 ± 0.06	47	72	120	685 ± 40
RGZ J144921.5+501945	1.26 ± 0.12 (0.60 ± 0.43)	2.21 ± 0.12 (0.50 ± 0.01)	40	40	75	365 ± 35
RGZ J150407.5+574918	1.30 ± 0.10	2.06 ± 0.13	47	34	80	480 ± 40
RGZ J150455.5+564920	0.93 ± 0.14	2.35 ± 0.05	43	97	140	720 ± 25
RGZ J151136.9+335501	0.76 ± 0.18	1.83 ± 0.13	43	34	75	520 ± 35
RGZ J152737.1+182250	1.35 ± 0.08 (0.50 ± 0.10)	2.07 ± 0.10	61	43	75	440 ± 45
RGZ J153421.4+333436	0.91 ± 0.11	2.18 ± 0.10	54	47	100	350 ± 20
RGZ J170002.6+270549	1.17 ± 0.15 (0.61 ± 0.44)	1.64 ± 0.17	33	27	60	440 ± 40

Note. f_{FR} is an index that quantifies FR morphology based on the position of the brightest feature in the source's lobe, calculated between the position of the optical host and farthest extent of the lobe and separately for each lobe of each radio galaxy (see Section 3.2 for details). Values quoted in brackets are for cases where the radio core dominates the lobe flux density. $\theta_{FRI/FRII}$ is the projected angular extent of either the FRI or FRII lobe, measured between the position of the host and outermost 3σ contours. θ_{total} is the projected total angular extent of the radio source measured between the outermost 3σ contours with an accuracy of 5 arcsec. The FIRST survey images are used for the size measurements unless stated otherwise. D_{total} is the total linear size of the source.
[a] NVSS survey used.

3.3. Optical Properties

The absolute magnitudes in the optical R band are rest-frame (k-correction performed using the online calculator[21] of Chilingarian et al. 2010; Chilingarian & Zolotukhin 2012). Spectroscopic observations are publicly available for nine candidates, as detailed in Table 1 and Section 3.1. Six hosts are quasars as classified in the SDSS database and Schneider et al. (1994). We measure emission lines of the remaining three hosts to classify them as either high- or low-excitation galaxies using the so-called excitation index EI (Buttiglione et al. 2010), where

$$\mathrm{EI} = \log_{10}\left(\frac{[\mathrm{O\ III}]}{\mathrm{H}\beta}\right) - \frac{1}{3} \times \left[\log_{10}\left(\frac{[\mathrm{N\ II}]}{\mathrm{H}\alpha}\right) + \log_{10}\left(\frac{[\mathrm{S\ II}]}{\mathrm{H}\alpha}\right) + \log_{10}\left(\frac{[\mathrm{O\ I}]}{\mathrm{H}\alpha}\right)\right]. \quad (2)$$

If EI > 0.95 the galaxy is classified as high excitation, otherwise as low excitation (Buttiglione et al. 2010).

We find the excitation indices EI = 1.44 (HERG) for RGZ J103435.8+251817, and EI = 0.50 (LERG) for RGZ J122425.8+020310. In the case of RGZ J1203 43.7+234305 the [N II], [S II], and Hα lines are not available, hence we use a simplified classification method from Best & Heckman (2012), which is based purely on the equivalent width of the [O III] line (EW). Specifically, Best & Heckman (2012) found that for EW([O III]) < 5 Å the galaxy is most likely low excitation. Likewise, Tadhunter et al. (1998) reported EW([O III]) > 10 Å for HERGs. We find EW([O III]) = 2.19 ± 0.58 Å for RGZ J120343.7+234304, and hence formally classify it as LERG. We also note that the spectrum of this galaxy in general lacks any strong emission lines, which strengthens its classification as a LERG. All line fitting parameters are taken from the SDSS DR13 database.

We also investigate in more detail the optical host of RGZ J123300.2+060325. The host is most likely a rare green bean galaxy (GBG; Schirmer et al. 2013). The GBGs are extended objects (Petrosian radius $r_{Petro} > 2''$) and have $g - r > 1.0$. The host of RGZ J123300.2+060325 has $r_{Petro} = 2''.61 \pm 0''.17$, and with colors $g - r = 1.02 \pm 0.04$, $r - i = 0.06 \pm 0.03$, $u - r = 2.36 \pm 0.20$, and $r - z = 0.57 \pm 0.05$ it is located in the region occupied by galaxies in Figure 2 of Cardamone et al. (2009), outside the selection requirement for green bean galaxies. The host colors meet 11 of 12 selection criteria for selection of GBGs proposed by Schirmer et al. (2013). We discuss this further in Section 4.2.

3.4. Citizen Scientists' Success Rates

Fifteen candidates are included in the RGZ DR1 catalog (O. I. Wong et al. 2017, in preparation; excluding the giant radio galaxies, which we deemed too difficult given the RGZ

[21] http://kcor.sai.msu.ru/

design since the large angular size of these two radio galaxies that extend well beyond the $3' \times 3'$ cut-out). Our candidates are all multi-component radio sources at the FIRST survey angular resolution, and for this reason they can appear multiple times in the RGZ catalog (one entry for each radio component). We assess each entry separately using two criteria: one, if the mid-IR host of the candidate HyMoRS was correctly identified, and two, if all radio components have been assigned to the overall radio structure of the source. Results are presented in Table 4.

For 12 candidates, all radio components have been correctly assigned by the citizen scientists (80% success rate). For 12 candidates the mid-IR hosts have been identified correctly by the citizen scientists (80% success rate). For 11 candidates the citizen scientists correctly assigned all radio components and identified the mid-IR host at the same time (73% success rate). Candidates with the multiple entries in the RGZ DR1 catalog, that have inconsistent classifications between the entries, are considered ambigous classifications (13%).

Complete radio component selection proved to be difficult for the citizen scientists in the case of multi-component radio sources with angular sizes of $\gtrsim 115''$. For radio galaxies of angular sizes $\leqslant 110''$ the success rates are 100% for the radio component association, and 90% for the mid-IR host selection (10% ambiguous). This result indicates that the main obstacle for the citizen scientists might have been the limited image size of the cut-outs they were presented with. For example, in the case of RGZ 120343.7+234305 ($4\farcm25$ angular size, 785 kpc linear size) the citizen scientists were presented with only the SE lobe, and as such they could not select the correct host nor identify all radio components of the whole radio galaxy. They did, however, correctly identify all lobe components of the SE lobe and correctly assigned no mid-IR host to it. Unfortunately, for any radio galaxy with angular size exceeding the RGZ cut-out size, this will almost always be the case, and thus the users of the RGZ catalog should be aware of this caveat to an otherwise valuable resource.

4. Discussion

4.1. The Origin and Formation of HyMoRS

The origin of the radio structure of HyMoRS is yet to be established. As favored by current consensus (e.g., Best 2009; Turner & Shabala 2015), radio morphology of radio galaxies is due to a combination of the radio source environment (nurture, Section 4.1.1) and jet power (nature, Section 4.1.2).

4.1.1. Nurture

As discussed in Section 1, there has been a wealth of studies of the FR dichotomy of radio galaxies. HyMoRS have been invoked as evidence for the significant environmental impact on the formation of radio morphology of radio galaxies (e.g., Gopal-Krishna & Wiita 2002; Meliani et al. 2008).

It has been suggested previously that radio galaxies may initially start as FRII radio sources (e.g., Kaiser & Best 2007), in which case an FRI morphology would form through the disruption and deceleration of the jets (Laing 1994; Meliani et al. 2008; Wang et al. 2011; Perucho et al. 2012; Turner & Shabala 2015, among others). Processes such as entrainment (Wang et al. 2011), and helical instability (Perucho et al. 2012), caused by interaction of lobes/jets with the surrounding media, and by density jumps in a nonuniform external medium Meliani et al. (2008), have been considered. Apart from Meliani et al. (2008), who focused specifically on theoretical modeling of HyMoRS, most of the deceleration models have been developed for the purpose of general discussion of the transition of FRII radio sources into FRIs. However, in the case of HyMoRS one needs to observe different radio morphologies on each side of a radio galaxy core. Assuming that the radio power of each of the twin jets is exactly the same, the deceleration would have to occur only on one side of the nucleus of the radio galaxy, indicating a highly asymmetric environment. Such asymmetric environments around radio galaxies have indeed been observed. For more discussion on the density asymmetry in the environments of radio sources see Section 4.2.

4.1.2. Nature

The observed morphology of a radio source in a two-dimensional image may suffer from persistent projection effects, causing the observed radio structures to represent projected and not intrinsic structures. Such effects include Doppler boosting (e.g., Blandford & Königl 1979; Orr & Browne 1982; Kellermann & Owen 1988; Hardcastle et al. 1998; Ubachukwu & Chukwude 2002), which may be particularly severe if the radio source is observed at a narrow angle to the line of sight.

The asymmetry in lobe lengths is sometimes used in the quantification of the projection angle, although we note that this will work only under a strong assumption that the jets are not intrinsically bent nor shortened due to differences in the environments on the twin jet paths. We find that 16% of candidates show no significant asymmetry in their lobe lengths, for 32% the longer arm (typically considered far side) is of FRI morphology, and for 52% the longer arm is of an FRII type. Furthermore, projection effects of intrinsically curved jets (e.g., in wide-angle tail radio galaxies) may also make sources appear asymmetric even without the presence of Doppler boosting. In this case, the hotspot of the near side may be projected to appear as knots or flare points, hence being classified as of FRI morphology, while the far lobe may appear as an FRII. The intrinsic asymmetry of lobes may be difficult to verify in the total intensity radio images of the radio sources. As shown by de Gasperin (2017), radio spectral maps and polarization imaging along the radio morphological classification are crucial in the confirmation of HyMoRS candidates and their intrinsic asymmetries.

HyMoRS can also be an intrinsically transient phenomenon, where it has been postulated that effects involving a combination of central engine modulation and differential light travel time between the approaching and receding parts of the radio source can shape the observed radio morphology (Gopal-Krishna et al. 1996). For example, Marecki (2012a) developed a simple model that can explain the observed morphological asymmetry in terms of the re-started activity of some radio galaxies (scenario (a)). Specifically, assuming that the radio source is at least at a moderate inclination to the observer's line of sight ($\lesssim 45°$), and the jet production is restarting within $(1–80) \times 10^4$ years, the differential light travel time effects may cause an apparent FRII morphology on one side (old), and FRI on the other (new), temporarily forming a HyMoRS from the observer's point of view. At least three known HyMoRS can be explained with this model based purely on their radio morphology (e.g., J1211+743, 3C249.1, 3C 334; Marecki 2012a, 2012b). Although the model was developed

Table 4
Candidate HyMoRS: RGZ DR1 Catalog Entries

HyMoRS Name	No. of Catalog Entries	Correct mid-IR Host Identified?	All Radio Components Included?	Consensus	Comments
RGZ J072406.7+380348	1	yes	no	57%	One radio component missing (outside RGZ cut-out).
RGZ J082231.1+531119	1	yes	yes	62%	
RGZ J085926.7+292738	1	yes	yes	100%	
RGZ J091408.0+522948	1	yes	yes	84%	
RGZ J094214.2+062751	1	yes	yes	86%	
RGZ J105521.2+372652	1	yes	yes	62%	
RGZ J120343.7+234205	1	no	no	55%	SE lobe only in the RGZ cut-out. Correctly assigned no IR host, but wrong host selection of the overall radio galaxy (see Section 3.4).
RGZ J123414.7+222248	1	yes	yes	52%	
RGZ J131414.1+020404	1	yes	yes	75%	
RGZ J144300.1+144042	3				Both lobes seen in the RGZ cut-outs.
	−a	no	no	71%	Only S lobe selected. Mid-IR object superposed within the lobe extent selected as host.
	−b	yes	yes	43%	
	−c	no	yes	70%	All radio components correctly identified as part of the radio galaxy, but radio galaxy incorrectly assigned no IR host.
RGZ J150407.5+574918	1	yes	yes	81%	
RGZ J151136.9+335501	2				
	−a	yes	yes	86%	
	−b	no	yes	78%	Incorrect host selected.
RGZ J152737.1+182250	2				
	−a	yes	yes	69%	
	−b	yes	yes	49%	
RGZ J153421.5+333436	1	yes	yes	84%	
RGZ J170002.6+270549	1	yes	yes	80%	

to cast doubt on hybrid radio morphology as an intrinsic property of some of the sources, perhaps at least a fraction of the HyMoRS population can be interpreted as a class of AGN transients (but see Cegłowski et al. 2013).

Here we also suggest two alternative scenarios when the AGN does not restart its radio activity, but instead (b) fully ceases the jet production or (c) is subject to increased activity (by e.g., undergoing a new accretion event, i.e., activity amplification). In the case of the jet switching off (b), and again invoking light travel arguments, we may observe FRII morphology on the far side, while the hotspot on the near side may have already faded away leaving behind only diffuse low level emission of a typical FRI morphology. Both scenarios, (a) and (b) assume the radio galaxy initially has an FRII morphology. For scenario (c) radio galaxy can be initially of either FRI or FRII morphology, where for the former we will observe a reversed structure to the one of scenarios (a) and (b).

4.1.3. Timescales

In the absence of the reacceleration of electrons, the hotspots will fade away on timescales of the order of $\sim 10^4$–10^5 years, while the diffuse lobe emission will be slowly radiating away for $>10^7$ years. The light travel time arguments of the source morphological asymmetry require modulation of activity on timescales of $\sim 10^5$–few $\times$ 10^6 years for physical scales of 100 kpc–1 Mpc. Hydrodynamical simulations of supermassive black hole temporal evolution (e.g., Novak et al. 2011; Gan et al. 2014) predict very chaotic accretion, with significant intermittency in accretion rate on a range of timescales, including bursts within a single accretion event (on orders of 10^6 years) and long-term activity intermittency with multiple accretion events (activity with timescales of $\sim 10^8$ years, separated by quiescent times of few $\times 10^7$ years). Timescales of $\sim 10^5$ years for the typical AGN phase (optical and X-ray regimes), and so the timescales of the variability of the supermassive black hole accretion rates, has also been suggested by Schawinski et al. (2015). Such timescales are in agreement with the differential light travel arguments put forward in Section 4.1.2.

4.2. HyMoRS as Quasars

Interestingly, 6 of 9 candidates with spectroscopic observations (20% of all our candidate HyMoRS) exhibit quasar properties. There is now a wealth of research that have shown that quasars are most likely triggered by mergers (e.g., Heckman et al. 1984; Bennert et al. 2008; Urrutia et al. 2008), have close companions (e.g., Disney et al. 1995) and may be residing in rich environments (Ellingson et al. 1991; Yee & Ellingson 1993, but see Wold et al. 2000; McLure & Dunlop 2001). We now know that radio loud quasars may be of both FR II (Ellingson et al. 1991; Yee & Ellingson 1993, and references therein) and FR I radio morphology (Heywood et al. 2007). Heywood et al. (2007) postulated that powerful radio sources may give rise to both radio morphological classes depending on the density of the environment in which the radio source expands. Confirmed HyMoRS whose hosts are quasars include J1348+286 (Gawroński et al. 2006) and 1004+130 (Gopal-Krishna & Wiita 2000), while the host of the archetypal HyMoRS, NGC 612 (Gopal-Krishna & Wiita 2000), is a Seyfert. The existence of HyMoRS quasars suggests that their environments may be very asymmetric. Furthermore, at least one of our candidates resides in a cluster evironment; RGZ J122425.8 +020310 is its cluster BCG. This further advocates the impact of rich environments on the radio morphology of HyMoRS.

On the other hand, the existence of HyMoRS green bean galaxies, which is rare on both accounts (there are only $\lesssim$20 HyMoRS not including candidates in this paper (e.g., Saikia et al. 1996; Gopal-Krishna & Wiita 2000; Gawroński et al. 2006; Pirya et al. 2011; de Gasperin 2017), and 22 GBGs known to date (Schirmer et al. 2013, 2016; Davies et al. 2015) suggests that modulation of central engine activity may be a non-negligible factor in the formation of hybrid radio morphology for at least some of the HyMoRS. The GBGs are ionization echoes of quasars experiencing a high activity episode and a subsequent rapid shut down. These galaxies are associated with shock or ionization fronts, including shocks of collimated jets heating the interstellar medium (Schirmer et al. 2013; Davies et al. 2015). We refer the reader to J. K. Banfield et al. (2017, in preparation) on the detailed analysis of GBGs and their radio properties.

It has been proposed that the AGN activity in GBGs has shut down within the last 10^4–10^5 years (Schirmer et al. 2013, 2016). RGZ J123300.2+060325 has no clear radio core detected down to the 3σ upper limit of 0.5 mJy, which suggests that the activity of the host is at most at low levels, if present at all. Furthermore, the projected linear extent of the RGZ J123300.2+060325 radio structure of 255 kpc indicates that its radio jets were launched at least 4 $\times$ 10^5 years ago, which might have coincided, or been directly related to, the high activity episode of the AGN immediately preceding the shut down. We suggest that RGZ J123300.2+060325 is a plausible example of the formation of HyMoRS through the amplification of the AGN activity, which we propose as an additional possible mechanism in this paper. This complements the central engine activity argument (activity cessation) put forward by Marecki (2012a, 2012b).

4.3. Radio Properties of HyMoRS and the Ledlow–Owen Diagram

Overall, our candidate HyMoRS are moderately powerful radio galaxies. In Figure 3(a), we plot the locations of the candidates in the Ledlow–Owen diagram. The Ledlow–Owen diagram (Owen & Ledlow 1994; Ledlow & Owen 1996) suggests a dependence of radio morphology on the absolute magnitude of the host of the radio galaxy. The dichotomy in radio morphology has been related to the optical brightness of the host through parameters such as black hole mass, pressure, and accretion rate, as all of these parameters can affect the jet propagation (Bicknell 1995; Ghisellini & Celotti 2001; Gopal-Krishna & Wiita 2001; Wold et al. 2007; Saripalli 2012).

In simple terms, one can also interpret the Ledlow–Owen separation line between FRIs and FRIIs as a change in intrinsic power of a radio galaxy, where FRIs are typically less powerful than FRIIs and thus their observed radio luminosity density is lower (but see Kapińska et al. 2012, for details on degeneracies between radio luminosity density and kinetic luminosity of jets, which lead to a nonstraightforward mapping between these two parameters). One could naively expect, therefore, that the weaker jets are more easily disrupted when expanding in a nonuniform external medium. Numerical simulations of Meliani et al. (2008), who attempted to model the disruption of only one of the twin jets by assuming a density jump in the external medium, show that weak jets (10^{36} W) can indeed efficiently form HyMoRS. However, they also show that for a right set of parameters (e.g.,

jet speed and density, and density ratio between the external dense medium and jet) hybrid radio morphology can also be formed in radio galaxies with powerful jets (10^{39} W). The fact that our candidate HyMoRS are located in the same region as powerful FRIIs (Figure 3(a)) suggests that the latter may be happening for at least some of the HyMoRS. The range of the observed radio luminosity densities of the candidate HyMoRS (Figure 3(b)), with a median $L_{\rm median} = 4.7 \times 10^{24}$ W Hz^{-1} sr^{-1} and a range of 3.4×10^{23}–6.7×10^{25} W Hz^{-1} sr^{-1}, seem to be in agreement with the results of Meliani et al. (2008).

Since the seminal study of Ledlow & Owen (1996), the classification of radio galaxies based on their optical spectra has been attracting more attention. Specifically, radio galaxies can be classified as either high excitation (quasar-mode) or low excitation (jet-mode; e.g., Laing et al. 1994; Best & Heckman 2012). The FRI/FRII classification cannot be directly mapped onto the HERG/LERG classification: while HERGs are typically powerful FRIIs, LERGs can be either FRIs or low power FRIIs. The low power FRII type radio galaxies occupy the FRI region in the Ledlow–Owen diagram (see, e.g., Best 2009; Miraghaei & Best 2017). In fact, based on Figure 5 in Miraghaei & Best (2017) it may seem that the separation occurs between the excitation classes rather than the morphological types of radio galaxies. A similar conclusion has recently been reached by Capetti et al. (2017) who used the same base data sample as Miraghaei & Best (2017), but see the discussion in Singal & Rajpurohit (2014) on the validity and Turner & Shabala (2015) on tightness of and environmental impact on the Ledlow–Owen correlation. Here, we find that our HyMoRS candidates can be both low- and high-excitation radio galaxies, though a study with larger number statistics is needed to understand how common each is.

Our sources display a range of linear sizes, from 175 kpc to megaparsec-scales, with two sources classified as giant radio galaxies (Figure 3(c)). The apparent scarcity of low luminosity and small linear size sources in our selection may be artificial, however; simply, we are less likely to select faint ($\lesssim$20 mJy) or small angular size sources ($\lesssim$30–40 arcsec) because the morphological classification becomes more ambiguous in those instances. This bias may also affect the distribution of HyMoRS in the Ledlow–Owen diagram (Figure 3(a)). Despite this, our current results already indicate a large diversity in both the type of host in which HyMoRS may reside and their radio properties. This suggests that, in principle, any active galaxy may be host to a hybrid morphology radio galaxy, and the morphology can be created by both the environment and central engine activity modulation.

5. Summary and Conclusions

We present the first 25 new candidates of HyMoRS drawn from the international citizen science project, RGZ, and its online discussion forum, the RadioTalk. For all the candidates, we provide mid-IR and optical hosts, redshifts, and radio and optical properties (luminosities, sizes). This is the first time such a large sample of candidate HyMoRS, with ancillary data on their hosts, has been collated. We discuss possible scenarios of the formation of hybrid morphology of radio galaxies, including,

(i) nonuniform environments,
(ii) cessation or amplification of the activity of the central black hole, and
(iii) Doppler boosting.

Detailed radio spectral and polarimetric analyses are needed to distinguish between these scenarios for each HyMoRS, but based on the available data, we postulate that HyMoRS are a diverse class of objects that, in principle, can be formed by any of these mechanisms and can be hosted by any active galaxy.

We cross-match our serendipitously selected candidate HyMoRS with the upcoming RGZ DR1 catalog to quantify the accuracy with which the citizen scientists identify and classify these complex sources. We find that the citizen scientists identify the correct mid-IR host in at least 80% of cases, and correctly identify all radio components of each radio galaxy in 80% of cases. For radio galaxies of angular sizes smaller than 115″, the success rates are 90% for the mid-IR host identification, and 100% for the radio component association. These results are very promising for future blind selection of candidate HyMoRS from the RGZ catalogs.

Given the rarity of these sources, and sheer volume of the data, we intend to pre-select all candidate HyMoRS from the FIRST survey using the RGZ project, for high-resolution continuum and polarimetric follow-up observations, and for efficient construction of future large HyMoRS samples. Deep follow-up studies of seven candidates presented here are currently in progress (A. D. Kapinska et al. 2017, in preparation). Future high-resolution all-sky surveys, such as NRAO VLA Sky Survey[22] (VLASS) which will have twice as high resolution as FIRST, will be of a particular value and great efficiency in the confirmation of the candidates. We highlight, however, the need for multi-resolution and/or multi-frequency radio data for at least some of the sources.

A.D.K. thanks P. A. Curran for constant encouragement in achieving academic goals.

This publication has been made possible by the participation of more than 11,000 volunteers in the Radio Galaxy Zoo Project. Their contributions are acknowledged at http://rgzauthors.galaxyzoo.org. We thank the following volunteers, in particular, for their comments on the manuscript or active search for candidate RGZ HyMoRS on RadioTalk: Jean Tate, Tsimafei Matorny, Victor Linares Pagán, Christine Sunjoto, Leonie van Vliet, Claude Cornen, Sam Deen, K.T. Wraight, Chris Molloy, and Philip Dwyer. Along with the contribution of the Radio Galaxy Zoo volunteers, we also acknowledge A. Kapadia, A. Smith, M. Gendre, S. George, E. Paget, R. Simpson, and C. Snyder who have made contributions to the project. The development of Radio Galaxy Zoo was supported by a grant from the Alfred P. Sloan foundation. A.D.K. and J.K.B. acknowledge financial support from the Australian Research Council Centre of Excellence for All-sky Astrophysics (CAASTRO), through project number CE110001020. S.S.S. thanks the Australian Research Council for an Early Career Fellowship (DE130101399). Partial support for this work for K.W.W. and L.R. was provided the U.S. National Science Foundation grant AST-1211595 and AST-1714205 to the University of Minnesota. K.S. acknowledges support from Swiss National Science Foundation Grants PP00P2_138979 and PP00P2_166159. F.d.G. is supported by the VENI research program with project number 1808, which is financed by the Netherlands Organisation for Scientific Research (NWO). H.A. benefitted from grant DAIP 980/2016-2017 of Univ. of Guanajuato.

[22] https://science.nrao.edu/science/surveys/vlass

This work made use of the FIRST and NVSS National Radio Astronomy Observatory (NRAO) Very Large Array (VLA) surveys. NRAO is a facility of the National Science Foundation operated under cooperative agreement by Associated Universities, Inc. This publication makes use of data products from the *Wide-field Infrared Survey Explorer*, which is a joint project of the University of California, Los Angeles, and the Jet Propulsion Laboratory/California Institute of Technology, funded by the National Aeronautics and Space Administration. Funding for the SDSS and SDSS-II has been provided by the Alfred P. Sloan Foundation, the Participating Institutions, the National Science Foundation, the US Department of Energy, the National Aeronautics and Space Administration, the Japanese Monbukagakusho, and the Max Planck Society, and the Higher Education Funding Council for England. The SDSS website is http://www.sdss.org/. This research has made use of the NASA/IPAC Extragalactic Database (NED), which is operated by the Jet Propulsion Laboratory, California Institute of Technology, under contract with the National Aeronautics and Space Administration. This research used TOPCAT—Tool for OPerations on Catalogues And Tables (Taylor 2005). Some of the data used in this paper were obtained from the Mikulski Archive for Space Telescopes (MAST). STScI is operated by the Association of Universities for Research in Astronomy, Inc., under NASA contract NAS5-26555. Support for MAST for non-*HST* data is provided by the NASA Office of Space Science via grant NNX09AF08G and by other grants and contracts.

ORCID iDs

A. D. Kapińska https://orcid.org/0000-0002-5289-5729
O. I. Wong https://orcid.org/0000-0002-2504-7628
H. Andernach https://orcid.org/0000-0003-4873-1681
F. de Gasperin https://orcid.org/0000-0003-4439-2627
C. J. Lintott https://orcid.org/0000-0001-5578-359X
Á. R. López-Sánchez https://orcid.org/0000-0001-8083-8046
R. P. Norris https://orcid.org/0000-0002-4597-1906
K. Schawinski https://orcid.org/0000-0001-5464-0888
B. Simmons https://orcid.org/0000-0001-5882-3323

References

Andernach, H., Jiménez Andrade, E. F., Maldonado Sánchez, R. F., & Vásquez Báez, I. R. 2012, in Science from the Next Generation Imaging and Spectroscopic Surveys (Garching: ESO), P1
Banfield, J. K., Wong, O. I., Willett, K. W., et al. 2015, MNRAS, 453, 2326
Baum, S. A., Heckman, T. M., & van Breugel, W. 1992, ApJ, 389, 208
Baum, S. A., Zirbel, E. L., & O'Dea, C. P. 1995, ApJ, 451, 88
Becker, R. H., White, R. L., & Helfand, D. J. 1995, ApJ, 450, 559
Bennert, N., Canalizo, G., Jungwiert, B., et al. 2008, ApJ, 677, 846
Best, P. N. 2009, AN, 330, 184
Best, P. N., & Heckman, T. M. 2012, MNRAS, 421, 1569
Bicknell, G. V. 1994, AuJPh, 47, 669
Bicknell, G. V. 1995, ApJS, 101, 29
Bilicki, M., Peacock, J. A., Jarrett, T. H., et al. 2016, ApJS, 225, 5
Blandford, R. D., & Königl, A. 1979, ApJ, 232, 34
Blandford, R. D., & Rees, M. J. 1974, MNRAS, 169, 395
Brescia, M., Cavuoti, S., Longo, G., & De Stefano, V. 2014, A&A, 568, A126
Buttiglione, S., Capetti, A., Celotti, A., et al. 2010, A&A, 509, A6
Capetti, A., Massaro, F., & Baldi, R. D. 2017, A&A, 601, A81
Cardamone, C., Schawinski, K., Sarzi, M., et al. 2009, MNRAS, 399, 1191
Cegłowski, M., Gawroński, M. P., & Kunert-Bajraszewska, M. 2013, A&A, 557, A75
Celotti, A., & Fabian, A. C. 1993, MNRAS, 264, 228
Chilingarian, I. V., Melchior, A.-L., & Zolotukhin, I. Y. 2010, MNRAS, 405, 1409
Chilingarian, I. V., & Zolotukhin, I. Y. 2012, MNRAS, 419, 1727
Collier, J. D., Banfield, J. K., Norris, R. P., et al. 2014, MNRAS, 439, 545
Condon, J. J., Cotton, W. D., Greisen, E. W., et al. 1998, AJ, 115, 1693
Dabhade, P., Gaikwad, M., Bagchi, J., et al. 2017, MNRAS, 469, 2886
D'Abrusco, R., Massaro, F., Paggi, A., et al. 2014, ApJS, 215, 14
Davies, R. L., Schirmer, M., & Turner, J. E. H. 2015, MNRAS, 449, 1731
de Gasperin, F. 2017, MNRAS, 467, 2234
De Young, D. S. 1993, ApJL, 405, L13
De Young, D. S. 2006, ApJ, 648, 200
Disney, M. J., Boyce, P. J., Blades, J. C., et al. 1995, Natur, 376, 150
Ellingson, E., Yee, H. K. C., & Green, R. F. 1991, ApJ, 371, 49
Fanaroff, B. L., & Riley, J. M. 1974, MNRAS, 167, 31P
Finkbeiner, D. P., Schlafly, E. F., Schlegel, D. J., et al. 2016, ApJ, 822, 66
Flewelling, H. A., Magnier, E. A., Chambers, K. C., et al. 2016, arXiv:1612.05243
Gan, Z., Yuan, F., Ostriker, J. P., Ciotti, L., & Novak, G. S. 2014, ApJ, 789, 150
Gawroński, M. P., Marecki, A., Kunert-Bajraszewska, M., & Kus, A. J. 2006, A&A, 447, 63
Gendre, M. A., Best, P. N., Wall, J. V., & Ker, L. M. 2013, MNRAS, 430, 3086
Ghisellini, G., & Celotti, A. 2001, A&A, 379, L1
Gopal-Krishna, & Wiita, P. J. 2000, A&A, 363, 507
Gopal-Krishna, & Wiita, P. J. 2001, A&A, 373, 100
Gopal-Krishna, & Wiita, P. J. 2002, NewAR, 46, 357
Gopal-Krishna, Wiita, P. J., & Hooda, J. S. 1996, A&A, 316, L13
Gorshkov, A. G., & Konnikova, V. K. 1995, AZh, 72, 291
Gregory, P. C., Scott, W. K., Douglas, K., & Condon, J. J. 1996, ApJS, 103, 427
Hardcastle, M. J., Alexander, P., Pooley, G. G., & Riley, J. M. 1998, MNRAS, 296, 445
Heckman, T. M., Bothun, G. D., Balick, B., & Smith, E. P. 1984, AJ, 89, 958
Heywood, I., Blundell, K. M., & Rawlings, S. 2007, MNRAS, 381, 1093
Hill, G. J., & Lilly, S. J. 1991, ApJ, 367, 1
Hurley-Walker, N., Callingham, J. R., Hancock, P. J., et al. 2017, MNRAS, 464, 1146
Jester, S., Schneider, D. P., Richards, G. T., et al. 2005, AJ, 130, 873
Kaiser, C. R., & Best, P. N. 2007, MNRAS, 381, 1548
Kapińska, A. D., Uttley, P., & Kaiser, C. R. 2012, MNRAS, 424, 2028
Kawakatu, N., Kino, M., & Nagai, H. 2009, ApJL, 697, L173
Kellermann, K. I., & Owen, F. N. 1988, in Galactic and extragalactic radio astronomy, Radio Galaxies and Quasars (Berlin: Springer-Verlag), 563
Komissarov, S. S. 1988, Ap&SS, 150, 59
Krause, M., Alexander, P., Riley, J., & Hopton, D. 2012, MNRAS, 427, 3196
Laing, R. A. 1994, in ASP Conf. Ser. 54, The Physics of Active Galaxies, ed. G. V. Bicknell, M. A. Dopita, & P. J. Quinn (San Francisco, CA: ASP), 227
Laing, R. A., & Bridle, A. H. 2002, MNRAS, 336, 1161
Laing, R. A., & Bridle, A. H. 2014, MNRAS, 437, 3405
Laing, R. A., Guidetti, D., Bridle, A. H., Parma, P., & Bondi, M. 2011, MNRAS, 417, 2789
Laing, R. A., Jenkins, C. R., Wall, J. V., & Unger, S. W. 1994, in ASP Conf. Ser. 54, The Physics of Active Galaxies, ed. G. V. Bicknell, M. A. Dopita, & P. J. Quinn (San Francisco, CA: ASP), 201
Laing, R. A., Riley, J. M., & Longair, M. S. 1983, MNRAS, 204, 151
Ledlow, M. J., & Owen, F. N. 1996, AJ, 112, 9
Lintott, C. J., Schawinski, K., Slosar, A., et al. 2008, MNRAS, 389, 1179
Lonsdale, C. J., Smith, H. E., Rowan-Robinson, M., et al. 2003, PASP, 115, 897
Marecki, A. 2012a, A&A, 544, L2
Marecki, A. 2012b, A&A, 545, A132
McLure, R. J., & Dunlop, J. S. 2001, MNRAS, 321, 515
Meier, D. L., Edgington, S., Godon, P., Payne, D. G., & Lind, K. R. 1997, Natur, 388, 350
Meliani, Z., Keppens, R., & Giacomazzo, B. 2008, A&A, 491, 321
Miraghaei, H., & Best, P. N. 2017, MNRAS, 466, 4346
Norris, R. P., Afonso, J., Appleton, P. N., et al. 2006, AJ, 132, 2409
Novak, G. S., Ostriker, J. P., & Ciotti, L. 2011, ApJ, 737, 26
Ofek, E. O., & Frail, D. A. 2011, ApJ, 737, 45
Orr, M. J. L., & Browne, I. W. A. 1982, MNRAS, 200, 1067
Owen, F. N., & Ledlow, M. J. 1994, in ASP Conf. Ser. 54, The Physics of Active Galaxies, The FRI/II Break and the Bivariate Luminosity Function in Abell Clusters of Galaxies, ed. G. V. Bicknell, M. A. Dopita, & P. J. Quinn (San Francisco, CA: ASP), 319
Perucho, M., Martí-Vidal, I., Lobanov, A. P., & Hardee, P. E. 2012, A&A, 545, A65
Pirya, A., Nandi, S., Saikia, D. J., & Singh, M. 2011, BASI, 39, 547

Planck Collaboration, Ade, P. A. R., Aghanim, N., et al. 2014, A&A, 571, A16
Proctor, D. D. 2011, ApJS, 194, 31
Rawlings, S. 2002, in IAU Symp. 199, The Universe at Low Radio Frequencies, ed. A. Pramesh Rao, G. Swarup, & Gopal-Krishna (Cambridge: Cambridge Univ. Press), 34
Reynolds, C. S., Di Matteo, T., Fabian, A. C., Hwang, U., & Canizares, C. R. 1996a, MNRAS, 283, L111
Reynolds, C. S., Fabian, A. C., Celotti, A., & Rees, M. J. 1996b, MNRAS, 283, 873
Saikia, D. J., Thomasson, P., Jackson, N., Salter, C. J., & Junor, W. 1996, MNRAS, 282, 837
Saripalli, L. 2012, AJ, 144, 85
Schawinski, K., Koss, M., Berney, S., & Sartori, L. F. 2015, MNRAS, 451, 2517
Scheuer, P. A. G. 1974, MNRAS, 166, 513
Scheuer, P. A. G. 1995, MNRAS, 277, 331
Schirmer, M., Diaz, R., Holhjem, K., Levenson, N. A., & Winge, C. 2013, ApJ, 763, 60
Schirmer, M., Malhotra, S., Levenson, N. A., et al. 2016, MNRAS, 463, 1554
Schneider, D. P., Schmidt, M., & Gunn, J. E. 1994, AJ, 107, 1245
SDSS Collaboration, Albareti, F. D., Allende Prieto, C., et al. 2016, arXiv:1608.02013
Singal, A. K., & Rajpurohit, K. 2014, Ap&SS, 353, 233
Tadhunter, C. N., Morganti, R., Robinson, A., et al. 1998, MNRAS, 298, 1035
Taylor, M. B. 2005, in ASP Conf. Ser. 347, Astronomical Data Analysis Software and Systems XIV, TOPCAT & STIL: Starlink Table/VOTable Processing Software, ed. P. Shopbell, M. Britton, & R. Ebert (San Francisco, CA: ASP), 29
Thorat, K., Saripalli, L., & Subrahmanyan, R. 2013, MNRAS, 434, 2877
Turner, R. J., & Shabala, S. S. 2015, ApJ, 806, 59
Ubachukwu, A. A., & Chukwude, A. E. 2002, JApA, 23, 235
Urrutia, T., Lacy, M., & Becker, R. H. 2008, ApJ, 674, 80
Wang, Y., Knigge, C., Croston, J. H., & Pavlovski, G. 2011, MNRAS, 418, 1138
Wen, Z. L., Han, J. L., & Liu, F. S. 2009, ApJS, 183, 197
Wold, M., Lacy, M., & Armus, L. 2007, A&A, 470, 531
Wold, M., Lacy, M., Lilje, P. B., & Serjeant, S. 2000, MNRAS, 316, 267
Wright, E. L., Eisenhardt, P. R. M., Mainzer, A. K., et al. 2010, AJ, 140, 1868
Yee, H. K. C., & Ellingson, E. 1993, ApJ, 411, 43
Zirbel, E. L. 1997, ApJ, 476, 489